WARWICK
THE UNIVERSITY OF WARWICK

Manuscript version: Author's Accepted Manuscript
The version presented in WRAP is the author's accepted manuscript and may differ from the published version or Version of Record.

Persistent WRAP URL:
http://wrap.warwick.ac.uk/171022

How to cite:
Please refer to published version for the most recent bibliographic citation information. If a published version is known of, the repository item page linked to above, will contain details on accessing it.

Copyright and reuse:
The Warwick Research Archive Portal (WRAP) makes this work by researchers of the University of Warwick available open access under the following conditions.

Copyright © and all moral rights to the version of the paper presented here belong to the individual author(s) and/or other copyright owners. To the extent reasonable and practicable the material made available in WRAP has been checked for eligibility before being made available.

Copies of full items can be used for personal research or study, educational, or not-for-profit purposes without prior permission or charge. Provided that the authors, title and full bibliographic details are credited, a hyperlink and/or URL is given for the original metadata page and the content is not changed in any way.

Publisher's statement:
Please refer to the repository item page, publisher's statement section, for further information.

For more information, please contact the WRAP Team at: wrap@warwick.ac.uk.

warwick.ac.uk/lib-publications

A Simple Mechanical Model for Steel Beam - Column Slab Subassembly Nonlinear Cyclic Behaviour

Tushar Chaudhari[1,a*], Gregory MacRae[2,b], Des Bull[2,c], G Charles Clifton[3,d] and Stephen J. Hicks[4,e]

[1]*Technical Manager - Structural Design, Neilsoft Limited, Pune, India*

[2]*Department of Civil and Natural Resources Engineering, University of Canterbury, Christchurch, New Zealand*

[3]*Department of Civil and Environmental Engineering, University of Auckland, Auckland, New Zealand*

[4] *School of Engineering, University of Warwick, Coventry, CV4 7AL, United Kingdom*

**corresponding author*

[a] tushar_dilip@yahoo.com, [b] gregory.macrae@canterbury.ac.nz, [c] des.bull@canterbury.ac.nz, [d] c.clifton@auckland.ac.nz, and [e] stephen.j.hicks@warwick.ac.uk

Keywords: Steel deck; Earthquake engineering; Mechanical model (strut and tie); Moment frames; Shear studs; Structural steel building with composite slab.

ABSTRACT

A simple strut-and-tie macro-model has been developed to represent the seismic behaviour of a composite deck slab, acting as part of a steel moment-frame beam-column-slab joint. The moment frame is subject to large lateral deformations, representing those from a strong earthquake, and yielding occurs at the beam ends. The frame sub-assemblies were modelled as elastic line elements connected with non-linear/linear spring elements. The model behaviour was compared to experimental test results. It was found that the model developed satisfactorily represented the envelope cyclic behaviour of the test frame sub-assembly with the different slab configurations. It is easy to implement in practice using widely used commercial software available to practising engineers.

Introduction

It is common practice to design composite deck floor slabs in steel buildings for gravity loads alone. However, during earthquake shaking of buildings with moment-frames, the slab may also increase the steel beam-column subassembly strength as a result of interaction between the slab and the steel elements. The increase in composite beam and subassembly strength can change the deformation mode from that anticipated into something undesirable, as noted by various researchers [1-6]. For example, in a subassembly designed for plasticity occurring at the beam ends, the presence of the floor slab makes the composite beam flexural strength greater than that of the steel beam alone, and column or panel zone yielding may occur instead of the anticipated beam yielding [3, 7-9]. This may lead to a higher probability of a soft-storey mechanism or other undesirable behaviour. However, the subassembly strength increase may be lost at large deformations due to slab degradation near the column. The increase in column demands due to slab interaction depends on the slab type (thickness, strength, confinement) and the connection to the column (touching outer flange, inner flange, or both). There are many different approaches to deal with the influence of the slab in design. Some engineers ignore it, while others consider the strength increase for column design as part of the overstrength considerations, but not for the design strength of the beam alone [10]. There is no universally agreed method to assess the strength, and provisions which do exist in Standards do not always provide a conservative result. Sometimes, in order to minimise the slab contribution on the composite beam overstrength of the column demand, a gap is placed between the slab and the column even though this introduces other issues/weaknesses into the system [11]. Given the lack of consistency of approaches and the non-conservative nature of some approaches.

A method is needed to assess column demands to safely design the sub-assembly using simple software readily available to engineers. The numerical model (finite element macro model) developed should represent the slab behaviour and be used in static pushover and THA (time history analysis). The model should consider:

a) the slab interaction on column exterior and interior faces (called as force transfer Mechanism 1 and 2 in Eurocode [12]),
b) shear stud characteristics and deck orientation, and
c) slab confinement in the slab-column interaction zone.

The prime focus of this research paper is to address the need above by developing a simple numerical model to predict column additional demands due to beam overstrength, caused by the slab-beam-column interaction in the composite slab construction [5, 8, 13]. In particular, answers are sought to the following questions:

i) What are the previous considerations for slab-frame interaction in seismic moment frames?
ii) Can a simple model be developed for readily available software which considers all likely failure modes?
iii) How well does the model work for slab detailing scenarios appropriate for practice?

Experimental Studies on Lateral Behaviour Composite Deck Slab and Steel Frame

Experimental tests of steel beam-to-column subassemblies (depicted in Figure 1), such as those by Lee and Lu [3], Civjan et al. [4], Leon et al. [14], Hobbs [15], Chaudhari [16], have shown that the presence of a slab connected to the beam, may increase the lateral strength to greater than that of the steel beam alone. In the Figure 1, it is assumed that the neutral axis on the left side beam is below the slab, so no gapping occurs at the bottom of the slab, however high neutral axis positions are also possible.

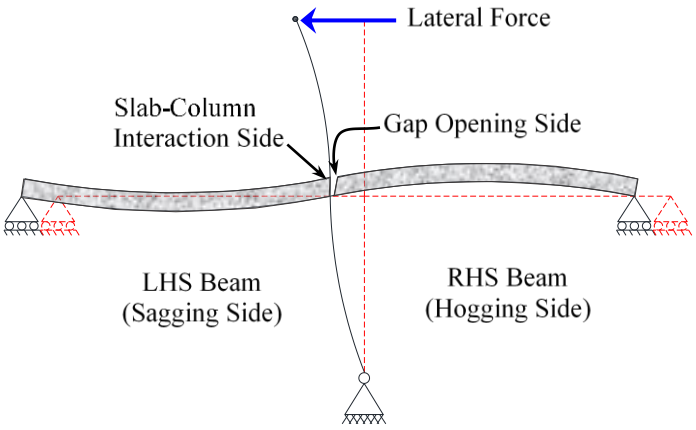

Figure 1- Frame Sub-assembly Subjected to Lateral Load.

The major mechanisms contributing to this strength increase results from direct bearing on the column outer flange, or on the inside of the column flanges. These have been called Mechanism-1 and Mechanism-2 in EN 1998-1 [12], as shown in Figure 2. An additional mode, caused by the slab pushing on the tops of the out-of-plane beams (i.e. beams perpendicular to lateral frame) causing beam twist, described as Mechanism-3 in EC8 [12], does not seem to have a significant influence on the strength in most subassemblies (Webb et al. [17]).

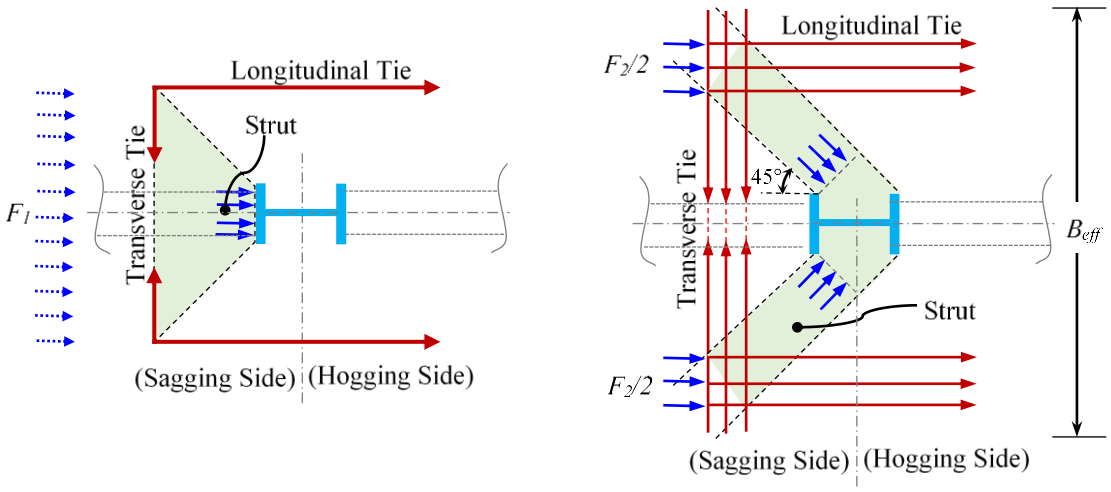

a) Mechanism-1: Direct Bearing onto Column Outer Flange

b) Mechanism-2: Compression on Column Sides

Figure 2 - Force Transfer Mechanisms between Slab and Column [12]

Experimental tests also showed that the increase in strength was often around 30% for standard slab details (Civjan et al. [4], Hobbs [15], Chaudhari et al. [18]) and that it was sensitive to the steel decking placement and details. For highly confined slabs beside the column, lateral

strength increases of up to 50% were obtained (Hobbs [15], Chaudhari [16]). There is the possibility that this increase in strength may cause yielding in a different, and possibly more undesirable, location than if there were no composite beam slab contribution (e.g. MacRae et al. [8]). This may lead to a higher probability of a soft-storey mechanism (such as seen by Yamada et al. [19]) or other unwanted behaviour. It has been observed that the post-peak strength degradation may occur due to concrete slab fracture between the flange tips (Civjan et al. [4], Chaudhari et al. [10], Hobbs [15]), or slab concrete longitudinal shear on either side of, and parallel to, the longitudinal beams (Hobbs [15]).

Hence, to avoid the strength increase (and possible subsequent decrease) in construction practice, a bearing of the slab on the column, which is common in conventional construction (e.g. Doneux and Parung [1], Hobbs [15], Chaudhari [16]) should be avoided. This may be accomplished by providing a gap between the slab and the column (Leon et al. [14], Hobbs [15], Chaudhari [16]). The gap may be filled with soft material (Chaudhari and MacRae [20]). However, the presence of the gap may lead to a greater possibility of column instability and buckling (Uang and Fan [21], FEMA451 [22]) and, as such, additional methods may be required to restrain this (Uang and Fan [21], MacRae and Clifton [23]).

Code Design Approaches

For design, slab in-plane effects are treated in different ways; some groups ignore the slab effect (e.g. ANSI/AISC:341-10 [24]). In New Zealand, the slab effect on the beam dependable strength is ignored for the design of the beam itself, but must be considered in the beam overstrength values used for the capacity design of the column and panel zone. The simple methodology, included in NZS3404:Part1:1997 [25], based on work by MacRae et al. [5], considers the tests of Civjan [2], the strut approach of Umarani and MacRae [26], and the fibre element modelling of the beam end by Kim et al. [27] for reinforced concrete frames. It results in an increase in strength of about 30% for some typical construction. This increase is less than the maximum obtained from more recent

steel building beam-column subassembly tests with composite deck flooring, where increases of up to 50% have been obtained (Hobbs [15], Chaudhari [16]). EN1998-1 [12] requires ductile reinforcement for the composite slab surrounding a column. To achieve steel section bottom flange yielding without slab concrete crushing, EN1998-1 [12] specifies that the total compressive force developed in the EC8 force transfer mechanisms should be 20% greater than the total slab force (due to positive and negative bending of the beams on either side of the column). However, an explicit method for column design considering slab-column effects is not specified.

In summary, ANSI/AISC:341-10 [24] ignores slab effects, while EN1998-1 [12] considers different force transfer mechanisms but does not explicitly describe the complete seismic design, and NZS3404:Part1:1997 [25] uses a simple method which applies to slab overstrength but and not to the beam design.

Numerical Approaches

Various numerical studies have also been conducted which consider slab-steel moment frame interaction effects for moment frames. For example, Kattner and Crisinel [28] developed a two-dimensional model using DIANA software to study the behaviour of semi-rigid composite joints, where beam elements represented the steel beam, column and the concrete slab. Shear studs were modelled using translational springs. The slab-column interaction was realised through the horizontal springs with a compression-only property acting only on the column outer flange without specific consideration of slab reinforcing. A linear kinematic condition was used to link the slab with the column, and the load-displacement behaviour of the shear stud translation springs was obtained from experiments and codes. These authors concluded that the proposed model of the composite joint with flush endplates could able to numerically simulate the global behaviour (i.e. moment-rotation) of the semi-rigid joint.

Rassati et al. [29] modelled partially restrained/semi-rigid composite connections using the equations in Annex J of the ENV1993-1-1 [30]. This model is formulated using eight different

springs to account for the influence of the various deformation components, including a slip in the bolts, partial interaction between the concrete slab and steel girder, shear deformation of the panel zone, and cracking and crushing of the slab. The model needs a user-defined element developed in ABAQUS software, but it is difficult for engineers to use in practice.

Umarani and MacRae [26] proposed a beam-column joint model to study the slab effect on the moment resting frames considering the beam growth caused by the gap opening as well as to study the effect on beam overstrength. To consider the slab effect a ‘slab element’ has been added; this element was modelled as a strut element with bilinear hysteretic behaviour. The beam-column joint was treated as a rigid joint; because of this, the shear deformation was ignored. Here, the slab element had some limitations, such as: the slab's bending effect was ignored; slab compressive resistance was considered to be elastoplastic, and interaction with the column sides was ignored as the slab was not connected with the column node. The proposed model developed using Ruaumoko – 2D [31], and calibrated with experimental results, captured the envelope behaviour for the models compared.

Elghazouli et al. [32] used a specialised non-linear finite element program ADAPTEC to study the seismic performance of a composite moment frame designed to the EN1998-1 [12] provisions. They conducted time-history analyses and showed that the seismic intensity and the panel zone parameters influence the behaviour. However, their main emphasis was not the slab behaviour.

Ikhlas S. Sheet et al. [33] improved the prediction by Umarani and MacRae [24] by using a Ramberg-Osgood hysteresis loop to better empirically predict the force-displacement unloading behaviour.

From the above, it may be seen that while various researchers have developed a beam-column joint model composed of linear and non-linear springs (representing the components like bolts, end plate, shear tabs, and panel zone), the modelling and calibration of these springs needs

specialised numerical software (like Opensees, Ruaumoko, ADAPTEC, and ABAQUS), which is not commonly used by practitioners.

Proposed Macro Model

Geometry idealisation

The moment frame internal beam-column sub-assembly with composite deck slab considered was based on the experimental tests of Chaudhari [16] as shown in Figure 3a. This subassembly was designed using capacity design principles to obtain strong column/connection–weak beam behaviour so that the column remains elastic. The model, developed using SAP2000 [32], considered an assemblage of non-linear springs, elastic beam-column elements, and slab axial elements to capture the behaviour caused by EC8 Mechanism-1 and 2 (EN1998-1 [12]). The 310UC158 column, 310UB32 beam, and 150mm thick ComFlor80 composite deck slab [34] were modelled with line elements along the centrelines of these elements, as shown in Figures 3b and c. The various nomenclatures given in the Figure 3 are, *'d'* the depth of steel beam, *'Hc'* depth of steel column and *'B_{eff}'* the effective width of slab.

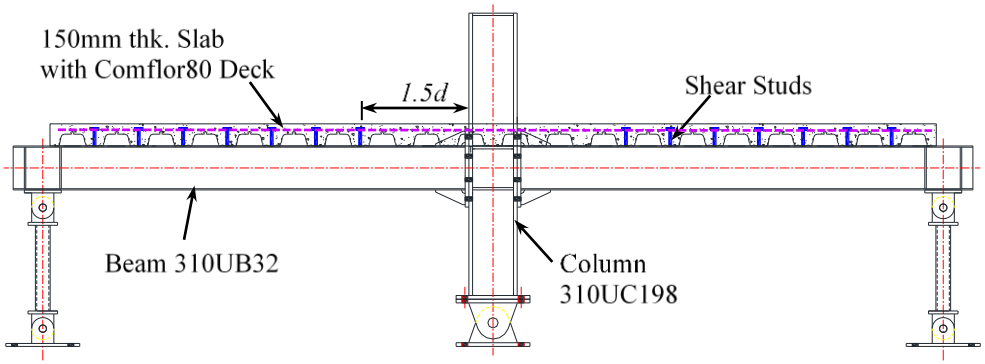

a) Experimental Test Setup

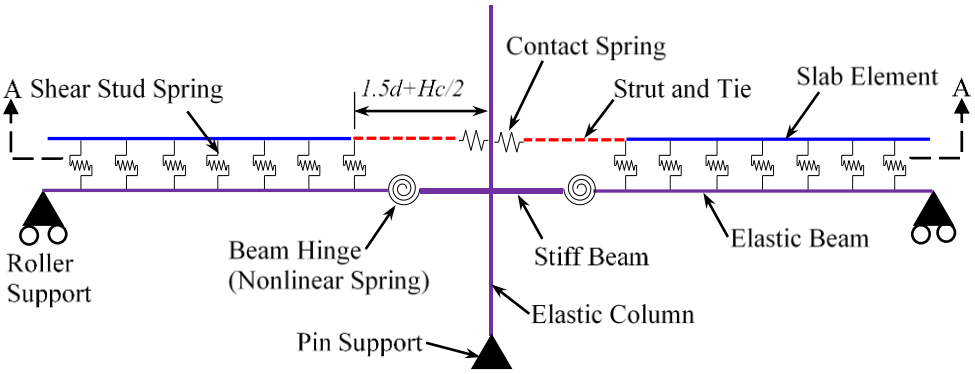

b) Schematic Representation of Numerical Model (Elevation)

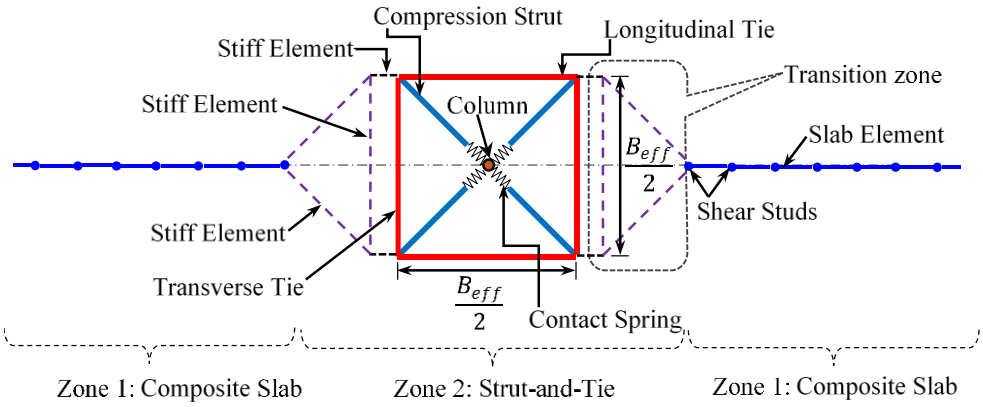

c) Schematic Representation of Numerical Model (Plan: Section A-A)

Figure 3 - Schematic Representation of Numerical Model.

Each beam was divided into three parts; (i) a stiff beam element (representing the joint, endplate and gusset plate connection), (ii) non-linear rotational springs (representing the beam plastic zone), and (iii) elastic beam elements (representing the elastic component) as shown in Figure 3b. Each shear stud was modelled with a non-linear spring using the SAP2000 [35] multilinear plastic link element. In current MRSF (moment resisting steel frame) design practice as per NZS3404:Part1:1997 [25] and AS/NZS:2327 [36], shear studs are not permitted between the column face and 1.5*d* from the column face, to minimise composite action in this zone thereby encouraging plastic hinging there, and also to mitigate the possibility of shear studs initiating cracking in the beam plastic hinge zone. Because of this, in the experiments and model, the first shear stud was located 1.5*d* from the column face, as depicted in Figure 3a.

The slab was divided into two zones, as shown in Figure 3c. The first zone (Zone 1) represents the slab near the shear studs. It was modelled as a line element connected by the shear stud springs to the beam element. The second zone (Zone 2) considers the slab from the column centreline to the first shear stud from the column. This was modelled as an assemblage of axial elements, as shown in Figure 3c. In the transition zone of Zone 2, stiff elements (shown as dashed) transfer force between the composite slab section (i.e. Zone 1 slab element) and the elements in the Zone 2 braced rectangular box arrangement shown in red and blue. The diagonal compression struts carry compression force from bearing between the slab and the inside and outside of the column flanges to the transition zone elements. The panel zone was assumed rigid based on an experimental study [16] and previous numerical study observations.

Concrete Constitutive Relationship

The concrete uniaxial compression model of Aslani and Jowkarmeimandi [37] was used; here, the compression envelope used the Carreira and Chu [38] concrete model, with exponential values for the ascending and descending branches. The compressive stress is provided as a tabular function of the plastic strain. In the current analysis, the uniaxial compressive stress-strain curve was assumed linear up to $0.4f'_c$. Thereafter it was calculated according to Equations 1 to 3, as shown in Figure 4a.

$$f_c = \frac{f'_c \, n \left(\varepsilon_c / \varepsilon'_c\right)}{n - 1 + \left(\frac{\varepsilon_c}{\varepsilon'_c}\right)^n} \tag{1}$$

$$n = n_1 = [1.02 - 1.17(E_{sec}/E_c)]^{-0.74} \quad if\ \varepsilon_c \leq \varepsilon'_c \tag{2}$$

$$n = n_2 = n_1 + (a + 28b) \quad if\ \varepsilon_c \geq \varepsilon'_c \tag{3}$$

where:

f_c = Compressive stress of concrete (MPa)

E_c = Tangent modulus of elasticity of concrete (MPa)

E_{sec} = Secant modulus of elasticity (MPa)

ε_c = Strain of concrete

f'_c = Cylinder compressive strength of concrete (MPa)

ε'_c = Tensile strain corresponding to tensile strength = $\left(\frac{f'_c}{E_c}\right)\left(\frac{r}{r-1}\right)$

n = Material parameter that depends on the shape of the stress–strain curve

n_1 = Modified material parameter at ascending branch

n_2 = Modified material parameter at descending branch

a = Constant = $3.5(12.4 - 0.0166f'_c(MPa))^{-0.46}$

b = Constant = $0.85\ exp(-911/f'_c\ (MPa))$

r = Constant = $(f'_c(MPa)/17) + 0.8$

The stress-strain relationship of concrete under tension was assumed to be linear up to the maximum tensile strength of concrete, f_{tu}, where f_{tu} (MPa) = $0.36\sqrt{(f'_c\ (\text{MPa}))}$ [39]. Thereafter the tensile strength decreased, as shown in Figure 4b. The concrete tensile stress-strain model is given in Equation 4 [37], where f_t is the concrete tensile stress, ε_t is the concrete tensile strain, f_{tu} is concrete tensile strength, and ε_{tu} is the strain corresponding to concrete maximum tensile strength.

$$\begin{aligned} f_t &= E_c\,\varepsilon_t && if\ \varepsilon_t < \varepsilon_{tu} \\ &= f_{tu}\left(\varepsilon_{tu}/\varepsilon_t\right)^{0.85} && if\ \varepsilon_t > \varepsilon_{tu} \end{aligned} \tag{4}$$

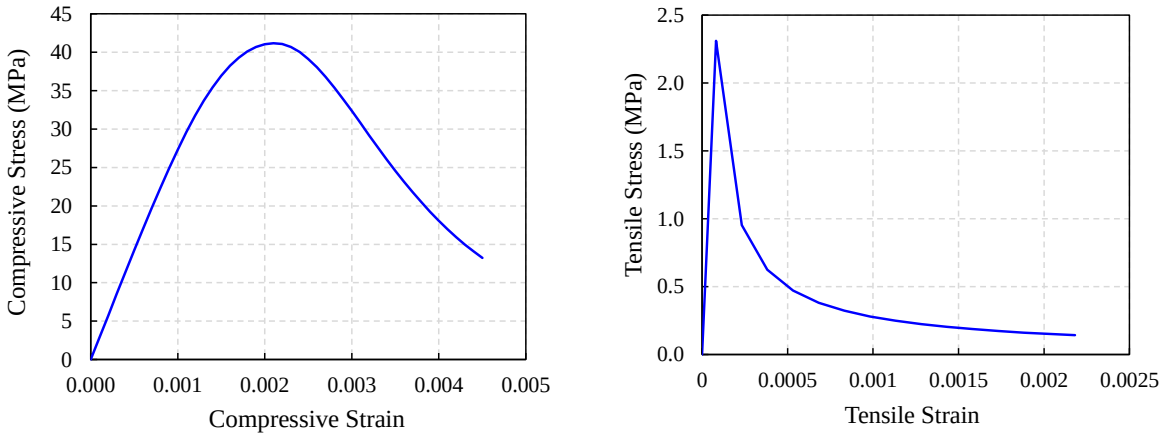

a) Compression Envelope Curve

b) Tension Envelope Curve

Figure 4 - Uniaxial Stress-Strain Curve of Concrete under Compression and Tension Loading

Coordinate system

In the global coordinate system used, the X-axis represents the longitudinal direction of beams, and the global Y-axis is orthogonal to the beam in the horizontal plane (representing the transverse

direction). The global Z-axis defines the vertical direction of the frame sub-assembly, which coincides with the longitudinal axis of the column, as shown in Figure 5a. The sectional and force-deformation properties for the various elements were provided in their local co-ordinate system [35]. This is denoted using 1, 2 and 3 as shown in Figure 5b.

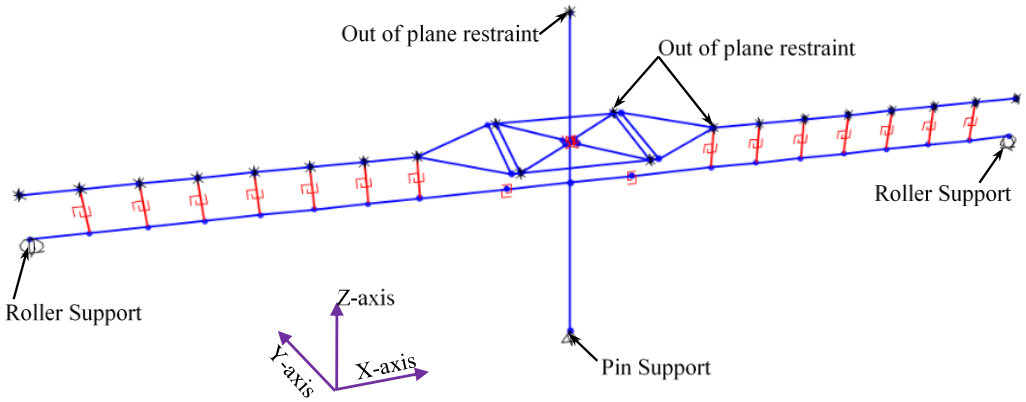

a) Sub-assembly Global Co-ordinate System and Boundary Conditions

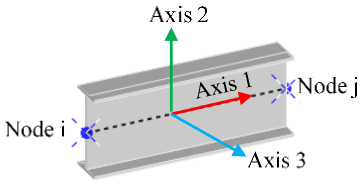

b) Member Local Co-ordinate System

Figure 5 - Numerical Model Co-ordinate System.

Element Formulation

Beam Element with Rotational Spring

The idealised numerical model of the frame sub-assembly's beam is shown in Figure 6, which was discretised in three parts (as mentioned before); stiff zone, plastic hinge zone, and the elastic beam. The beam-to-column connection was considered as a stiff zone (based on the experimental observations). Also, to simplify the model, the endplate connection and gusset plates were treated as a stiff beam element. The moment of inertia for the stiff beam element was calculated as the sum of the moment of inertias of the bare beam and the gusset plates (i.e. $I_{stiff} = I_{beam} + I_{gusset}$).

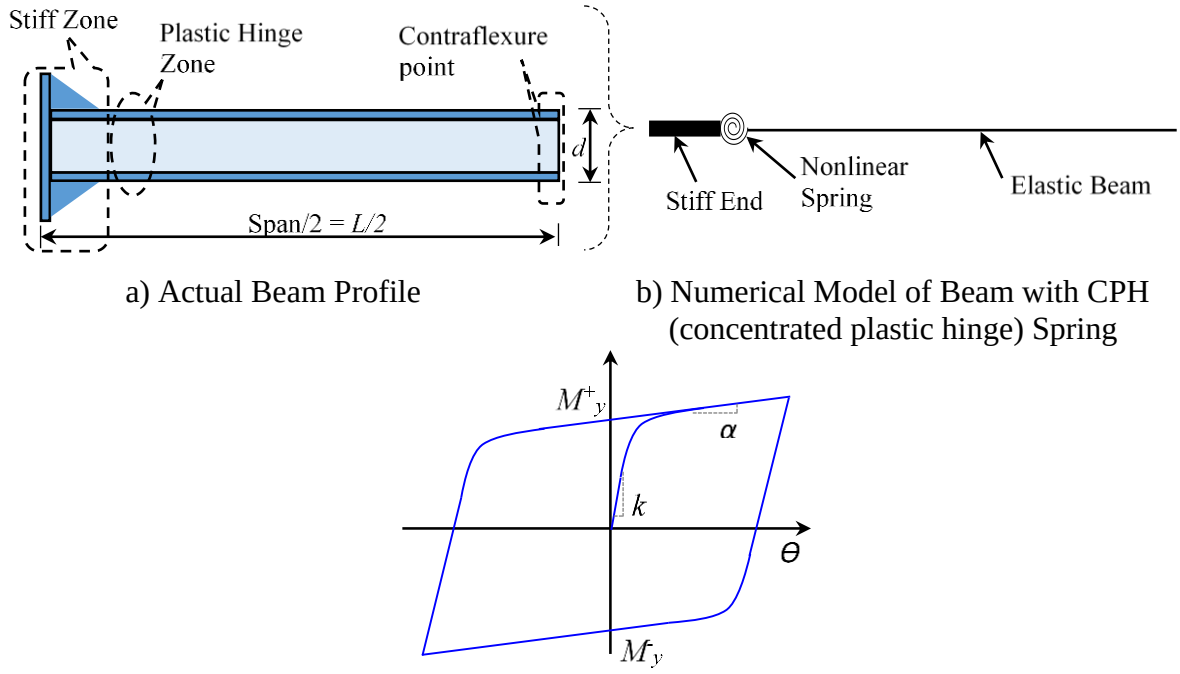

a) Actual Beam Profile

b) Numerical Model of Beam with CPH (concentrated plastic hinge) Spring

c) CPH Spring (Hysteresis behaviour of non-linear spring)

Figure 6 - Beam Element Details

The nonlinearity of the beam was simulated using the CPH (concentrated plastic hinge) approach; hence a zero-length non-linear link element was used in the beam plastic hinge region. The non-linear cyclic behaviour was simulated using the SAP2000 [35] Wen plasticity model. The non-linear spring degrees-of-freedom are: (i) axial deformation in translational direction 1 (i.e. U1) with linear properties, (ii) shear deformation in translational directions 2 and 3 (i.e. U2 and U3 respectively) with linear properties, (iii) rotation in direction 3 (i.e. R3) with non-linear properties, and rotational deformation restraint in directions 1 and 2 (i.e. R1 and R2). A high axial stiffness and shear stiffness were provided. These stiffnesses were made high enough so the results were not sensitive to the actual values, but low enough to avoid numerical instability problems.

The input properties required for the Wen plasticity spring are; (i) initial flexural stiffness, (ii) post-yield stiffness ratio, (iii) yield moment, and (iv) exponent coefficient. The initial flexural stiffness of the rotational spring (K_{spring}) was calculated using Equations 5 and 6, where I_{mod} is the modified moment of inertia of the beam, I_{beam} is the beam moment of inertia about the major axis, and n is the multiplication factor of 10 based on Ribeiro et al. [40], and this represented the data.

$$K_{spring} = \text{n}.\frac{6.E.I_{mod}}{L_1} \quad (5)$$

$$I_{mod} = I_{beam}.\frac{\text{n}+1}{\text{n}} \quad (6)$$

The initial flexural stiffness of the rotational spring was modified by a constant 'n' to account for the combined effect of the non-linear springs and the elastic beam-column element. The rotational spring at the beam end was modelled as a rigid-plastic (by multiplying initial stiffness with 'n') so that the numerical model does not pose any numerical instability issues [40].

As reported by Ibarra and Krawinkler [41], the overall hysteretic response of the beam is a combination of the individual moment-rotation of the rotational spring and the elastic beam-column element. In the non-linear time history analysis, the rotational spring dominates the overall moment-rotation behaviour of the beam, and the beam-column element remains elastic. Since the rotational spring and the elastic beam-column element are connected in series, the post-yielding to elastic stiffness ratio (i.e. the strain hardening coefficient) was adjusted to obtain the strain hardening coefficient of the rotational spring. The methodology suggested by Ribeiro et al. [40] was adopted here to obtain the strain hardening coefficient of the rotational spring. The post-yield stiffness ratio of the rotational spring was calculated as:

$$\alpha_{spring} = \frac{\alpha}{1+[n.(1-\alpha)]} \quad (7)$$

Where 'α' is the nominal strain hardening ratio, which was considered equal to 3% (this value was assumed based on the literature and the section analysis of the beam 310UB32), the post-yield stiffness ratio of the rotational spring α_{spring} was equal to 0.0028 (for n = 10). This value was used in the current numerical simulation. Isotropic hardening was considered by increasing the predicted plastic moment, M_p, to the likely maximum moment, M_m using the methodology suggested by Kawashima et al. [42]. The flexural strength, M_m, is calculated as $Z_p(\sigma_u + \sigma_y)/2$, where σ_y is the tension coupon test yield stress, σ_u is the tension coupon test ultimate tensile stress, and Z_p is the section plastic modulus, which accounts for isotropic hardening. In the Wen plasticity model, the sharpness of the hysteresis was influenced by the yielding exponent coefficient.

Shear Stud Idealisation

In the numerical model, the shear stud is represented using a non-linear link element available in SAP2000 [35]. The force-displacement behaviour of the shear studs was obtained from the methodology reported in the literature [43-45]. In the current numerical simulation, the force-displacement relationship for the shear stud was calculated using the Johnson and Molenstra [46] formulation,

$$P=P_{rk}(1-e^{-\beta s})^{\alpha} \quad (8)$$

where 'P_{rk}' is the characteristic strength of the shear studs, which was calculated based on the research study conducted by HERA [45], the values for constants 'α' & 'β' were selected as 0.989 and 1.535mm^{-1} respectively as specified by Johnson and Molenstra [46]. The resulting shear stud non-linear load-slip behaviour is shown in Figure 7. The use of the shear stud spring element is simple and gives good convergence [47]. The shear spring idealisation is from the beam mid-height to the mid-thickness of the topping concrete, as shown in Figure 7 (b). Rigid constraints assigned in the respective axes of the link element allow the shear stud force-slip relationship to represent the slip between the top of the steel beam and the concrete decking. Shear spring characteristics have been modified to represent the two shear studs placed beside each other. The various nomenclature given in the Figure 7 are, *'t_c'* topping slab thickness, *'h_{rc}'* height of steel deck rib.

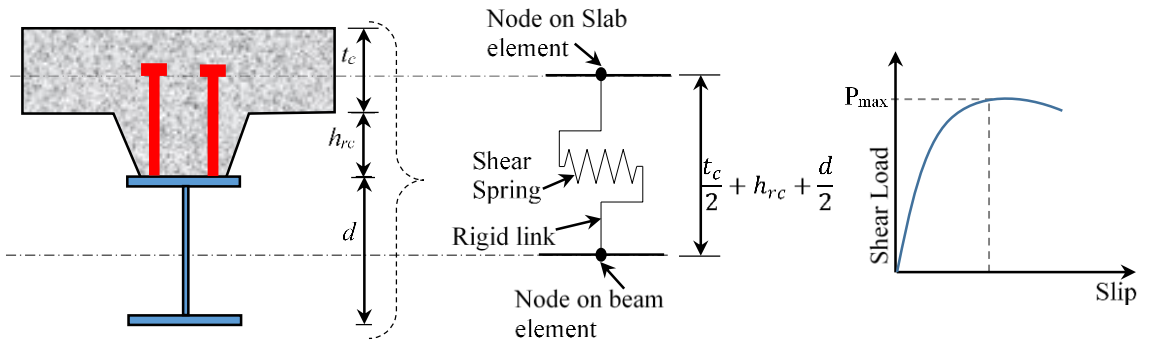

a) Shear Stud b) Analytical model c) Load-Slip Envelope

Figure 7 - Non-linear Shear Spring to Model the Behaviour of Shear Stud.

Slab-Column Interaction Idealisation

The strut-and-tie formulation at the slab-column interaction zone considers that both force transfer mechanisms (1 and 2) act in parallel as shown in Figure 8. In the proposed model, they were represented by an equivalent compression strut *'k_{eq}'* with the stiffness of a combined strut ($k_{eq} = k_1 + k_2$), where *'k_1'* and *'k_2'* are the axial stiffness for Mechanism 1 and 2 respectively. Therefore, the equivalent strut is represented by a single compression strut with an area equal to sum of those from the Mechanism 1 and 2.

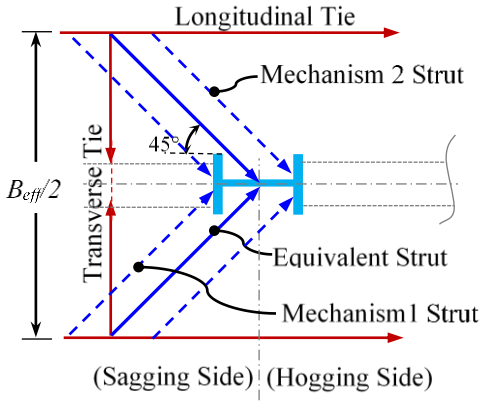

Figure 8 - Equivalent Strut comprising of Mechanism 1 and 2 struts.

This equivalent compression strut was assumed to act at the inclination of 45° and connected to the column centre line with the non-linear compression-only contact spring shown in Figure 9, representing the slab-column interaction. The struts extend to $B_{eff}/4$ in the slab longitudinal and transverse directions, where B_{eff} is slab effective width equal to $L/4$, where L is the distance between column centres in the longitudinal direction according to NZS3404 [25]. The effective width of the slab (B_{eff}) represents the region of collection of slab force. However, the strut and tie model, $B_{eff}/2$ are placed halfway along this collection region. The various nomenclatures given in the Figure 9 are, *'L_{strut}'* the length of strut, *'A_{strut}'* the area of strut, *'F_T'* the force in transverse tie, *'F_L'* the force in longitudinal tie, *'F_c'* the force in equivalent compression strut.

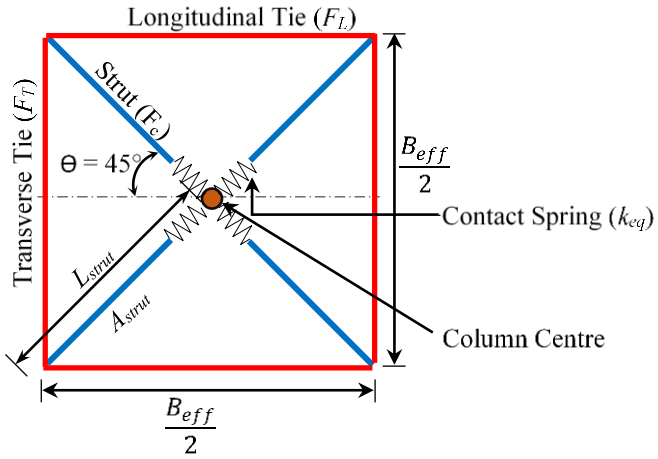

Figure 9 - Idealised Strut-and-Tie model.

The non-linear contact spring force-displacement properties used the concrete compression stress-strain envelope in Figure 4. Here, the compression force, F_c, was obtained as the stress, f_c, multiplied by the strut area, A_{strut}. The corresponding displacement, Δ_{strut}, was the corresponding concrete strain, ε_c, multiplied by the strut length, L_{strut}. The contact spring force-displacement relationship is shown in Figure 10. Here, the peak of the force-displacement envelope of compression only non-linear contact spring reparents bearing/crushing failure and was obtained as the maximum compression stress ($f_{c,max}$) multiplied by the strut area (A_{strut}).

The deck orientation effect has been considered while calculating the force-displacement properties of the non-linear contact spring. In the transverse deck assembly, the column only bears against the topping concrete, while for a longitudinal deck slab, the concrete in the decking trough may also contribute to the bearing area. This aspect is considered in the current model while calculating the slab contact area.

In case of the full depth slab sub-assembly, the concrete in around the column in full depth portion was confined using a reinforced cage. The effect of the concrete confinement is considered while determining the non-linear contact spring properties using stress-strain properties of confined concrete based on the Mander et al. [48] confined concrete model.

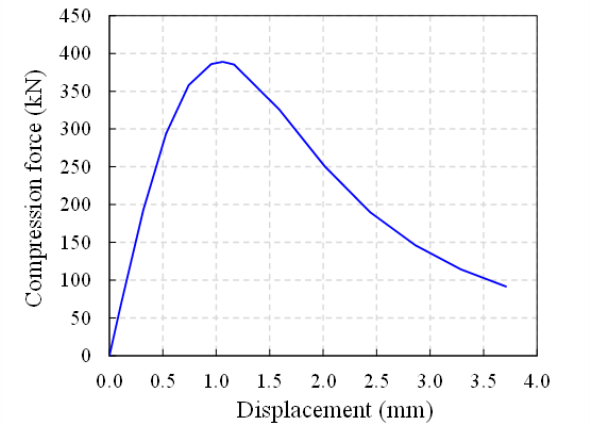

Figure 10 - Contact Spring: Force-Displacement Envelope

In between the composite slab section (zone-1) and the strut-and-tie (zone-2), the transition zone was connected through the series of rigid axial elements, with the cross-sectional area, $A_{stiff} = B_{eff}/2.t_c$, as shown in Figure 3. The slab in the composite section region was linear elastic flexural with an upper limit on tensile strength (F_{ten}) and it then immediately loses its strength after cracking, as shown in Figure 4b. Here, $F_{ten} = f'_{ct}A_s$ where f'_{ct} is maximum tensile stress (i.e. $0.36\sqrt{f'_c}$, here f'_c is in MPa) and 'A_s' is the effective slab area ($B_{eff}t_c$). The steel reinforcing in this region was ignored for simplicity. The struts in the slab-column interaction zone have compression-only properties, whereas the tie members carry tension only. Both the transverse and longitudinal tie members were assumed linear elastic with the stiffness properties of the rebars.

Boundary Conditions and Loading Protocol

To replicate the boundary conditions of the tested frame subassembly, the beam ends were provided with roller supports and the column bottom with pinned supports. Shear studs, and the corners of strut-and-tie elements, were provided with out-of-plane restraints to avoid numerical instability as depicted in Figure 5a. The displacement control loading protocol specified in ACI T1.1-01 [49] (refer Figure 11) was applied to the column top as per the experimental tests.

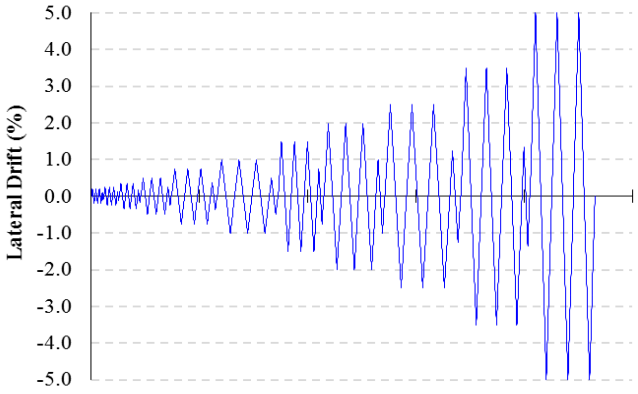

Figure 11 – Displacement Control Loading Regime

Validation of Proposed Model

As part of the experimental research, beam-column subassembly tests with different slab configurations were conducted at the University of Canterbury [10, 16]. Specimen details are summarised in Table 1 and shown in Figures 12 to Figures 16.

Table 1: Details of Experimental Test Configurations

Test	Specimen Designation	Deck Orientation	Detail around the Column	Active Force Transfer Mechanism
1	Bare Steel Frame **(BSF)**	-	-	-
2	Fully Isolated Slab Unit **(FI-SU)**	Transverse Deck	All around isolation of slab from the column	none
3	Shear Key Slab Unit **(SK-SU)**	Longitudinal Deck	Slab isolated on the column outer flange	Mechanism-2
4	Modified Shear Key Slab Unit **(MSK-SU)**	Longitudinal Deck	Slab isolated on the column outer flange	Mechanism-2
5	Full Depth Slab Unit **(FD-SU)**	Transverse Deck	Slab casted touching to the column on full depth	Mechanism-1 and -2

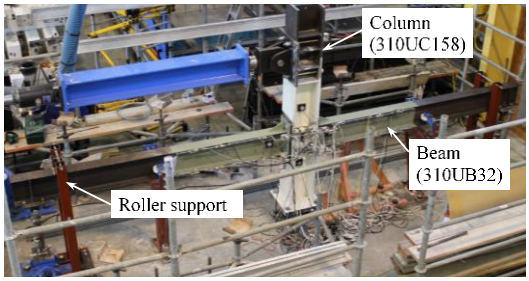

a) Test configuration setup

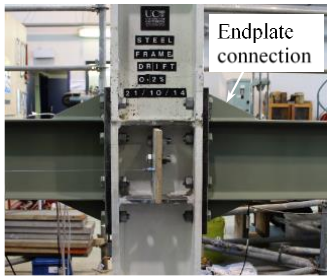

b) Connection details

Figure 12 – Bare Steel Frame (BSF) Test Sub-Assembly

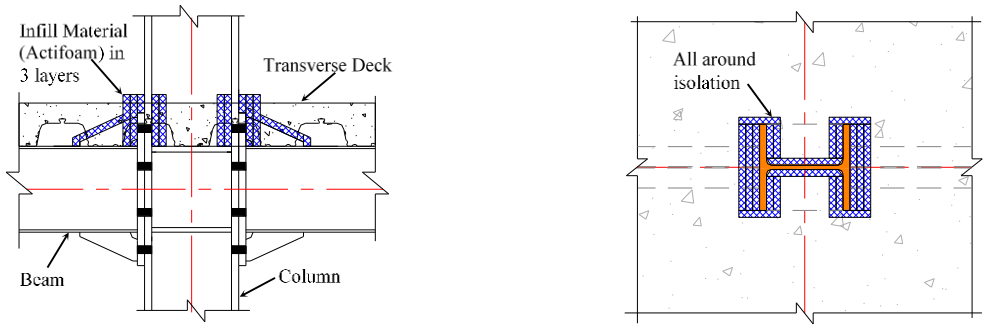

a) Front view b) Plan

Figure 13 – Fully Isolated Slab Unit (FI-SU) Test Sub-Assembly

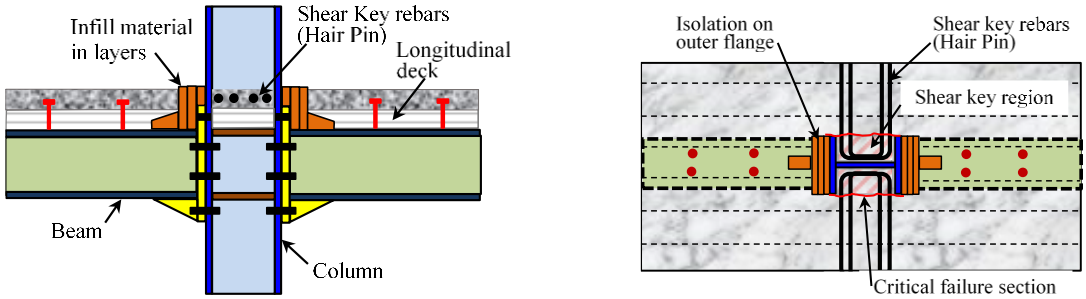

a) Front view b) Plan

Figure 14 – Shear Key Slab Unit (SK-SU) Test Sub-Assembly

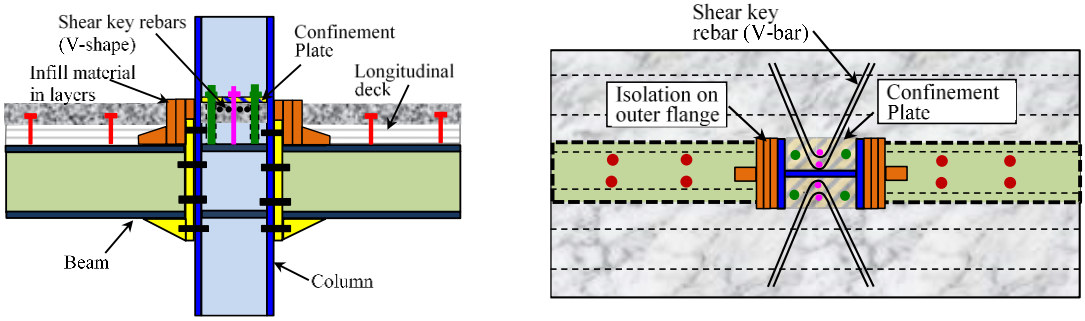

a) Front view b) Plan

Figure 15 – Modified Shear Key Slab Unit (MSK-SU) Test Sub-assembly

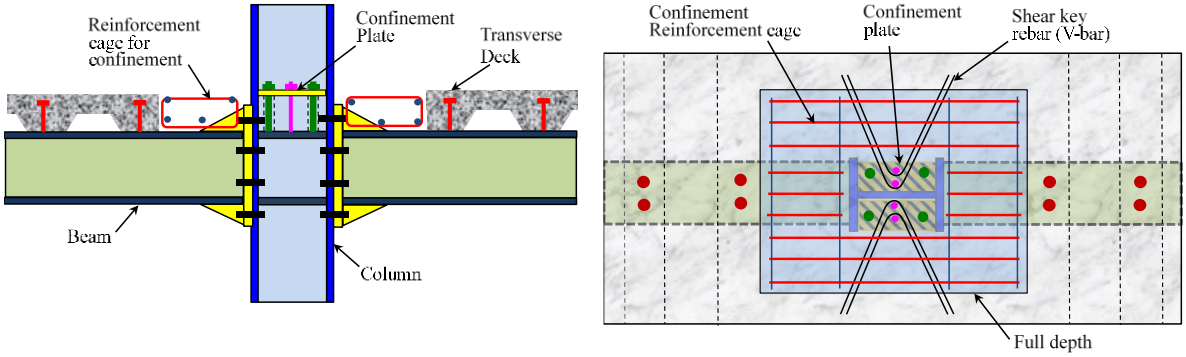

a) Front view b) Plan

Figure 16 – Full Depth Slab Unit (FD-SU) Test Sub-Assembly.

The comparison of the overall hysteresis behaviour of the frame sub-assemblies with different slab configurations obtained using SAP2000 [35] based numerical macro model with the

corresponding experimental test results are shown in Figure 17. It can be observed that the numerical model was able to simulate the cyclic behaviour of the frame sub-assembly with the different slab configurations with reasonable accuracy. Also, the numerical model captured the initial lateral stiffness. This is also summarised in Table 2. The deviation in the hysteresis loop of the BSF frame sub-assembly is shown in Figure 17a. This is due to the limitation of the non-linear spring. It fails to capture the full Bauschinger effect and beam buckling effect as observed in the experimental test. However, the developed numerical model simulates the key envelope behaviour of the FI-SU (Fully Isolated Slab Unit), SK-SU (Shear Key Slab Unit), MSK-SU (Modified Shear Key Slab Unit), and FD-SU (Full Depth Slab Unit) frame assemblies [10], as shown in Figure 17b to 17e.

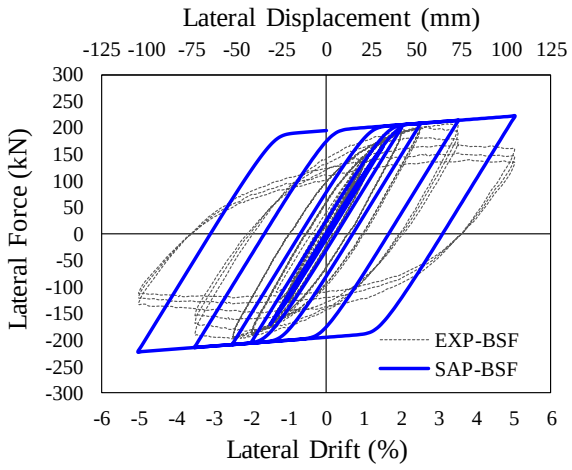

a) Bare Steel Frame

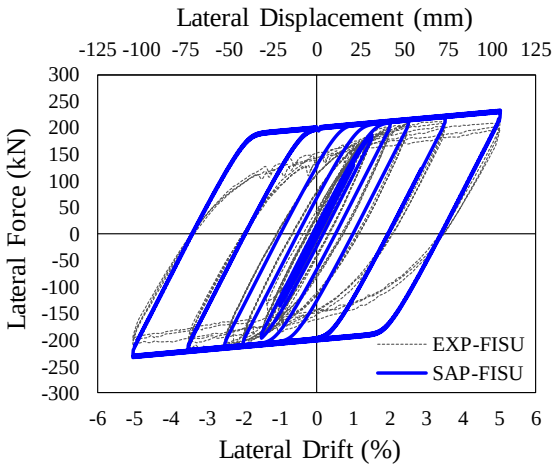

b) Fully Isolated Slab Unit

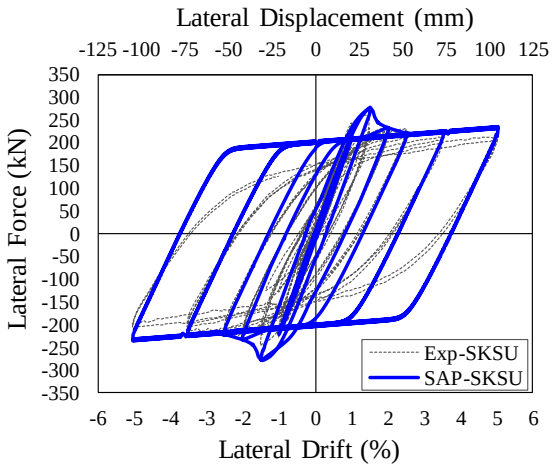

c) Shear Key Slab Unit

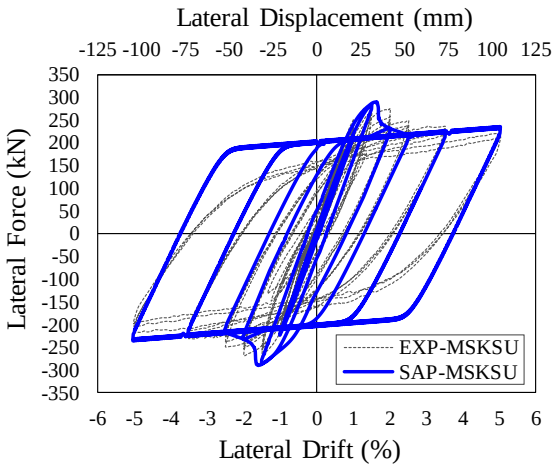

d) Modified Shear Key Slab Unit

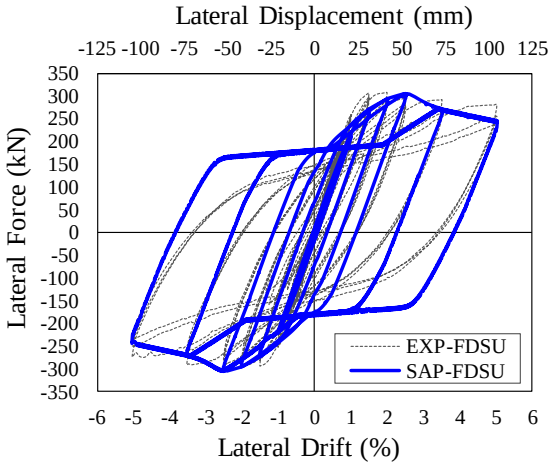

e) Full Depth Slab Unit

Figure 17 - Comparison of Numerically Simulated Hysteresis Plots with Test Results

Table 2: Comparison of Sub-assemblies Initial Stiffness and Peak Strength of Numerical Macro Model with Experimental Results

Test Specimen	Initial Stiffness (kN/m)			Peak Strength (kN)		
	Numerical (N)	Experimental (E)	Deviation (N-E)/E (%)	Numerical (N)	Experimental (E)	Deviation (N-E)/E (%)
Bare Steel Frame **(BSF)**	6212	6156	+1.0	214.1	206	+4
Fully Isolated Slab Unit **(FI-SU)**	7879	8747	-10	219.0	211.4	+4
Shear Key Slab Unit **(SK-SU)**	13183	15031	-12	277.6	263	+6
Modified Shear Key Slab Unit **(MSK-SU)**	13283	14506	-8	271.9	285.2	-5
Full Depth Slab Unit **(FD-SU)**	13298	16402	-19	326.7	306.3	+7

From above it can be seen that the strength deviation is about 7%. This is because of the assumptions made in the model and the inability to accurately assess material properties for the whole slab and beam elements. The stiffness deviation is between 8% to 12% for three slab assemblies and 19% for full-depth slab assembly. The numerical model did not consider the struts

at the beam ends, or slop beside the pins in the loading system. Also, the non-linear nature of stress-strain properties of concrete material as well as the concrete cracking, influences the stiffness estimation for the concrete elements. The stiffness of test specimens with slabs are greater than that of the numerical analysis, this is because of the stiffness of experimental tests was computed in the initial cycles with little cracking, while full cracking is assumed in the numerical model since the cracked slab properties were considered. This difference is likely to be more significant in the case of the full depth slab, where slab depth and concrete area is larger.

Conclusions

A simple model is developed for steel beam-column joints with slabs using readily available computer software, such that engineers can use in PBEE (performance-based earthquake engineering) time history analysis assessments due to earthquake excitation. The following conclusions are made:

(1) A number of tests on steel beam-column moment frame subassemblies with composite slabs indicate that the bare steel frame strength was increased up to 50% due to the presence of the slab (full-depth slab configuration) and this effect is often not considered in the routine design.

(2) The macro-model can reasonably predict the frame sub-assembly lateral strength and initial lateral stiffness. Specific considerations for the concrete bearing surface, shear stud characteristic, slab confinement are made. It is shown that the approach represents the behaviour of a number of subassemblies. However, there is some variation due to the model simplicity, consideration of the boundary conditions and the concrete cracking effects.

(3) The model captures the overall beam-column slab subassembly experimental envelope behaviour under cyclic loading well for slabs detailed in five different ways. The configurations involved: no composite slab; typical slab details; a highly confined slab; and

two other intermediate cases. Overall, the approach developed is good for use by practitioners.

Acknowledgements

The authors would like to acknowledge the MBIE Natural Hazards Research Platform for its support to conduct the proposed research study as a part of the Composite Solution Research Project. Additional support was provided by ComFlor New Zealand, John Jones Steel Research Funding, and Heavy Engineering Educational and Research Foundation (HEERF). All opinions expressed remain those of the authors.

References

[1]. Doneux, C. and H. Parung (1998)."A study on composite beam-column subassemblages." Proceedings of the 11th ECEE Conference, Paris.
[2]. Civjan, S.A. (1998). "Investigation of retrofit techniques for seismic resistant steel moment connections." Doctor of Philosophy, The University of Texas, Austin.
[3]. Lee, S.-J. and L.-W. Lu (1989). "Cyclic tests of full-scale composite joint subassemblages." Journal of Structural Engineering, 115(8), 1977-1998.
[4]. Civjan, S.A., et al. (2001). "Slab effects in SMRF retrofit connection tests." Journal of Structural Engineering, 127(3), 230-237.
[5]. MacRae, G.A., et al. (2007)."Overstrength effects of slabs on demands on steel moment frames." Pacific Structural Steel Conference 2007.
[6]. Plumier, A. and C. Doneux (2001). "Seismic behaviour and design of composite steel concrete structures." ECOEST2 and ICONS, LNEC Lisboa, Portugal.
[7]. Braconi, A., et al. (2010). "Seismic behaviour of beam-to-column partial-strength joints for steel–concrete composite frames." Journal of Constructional Steel Research, 66(12), 1431-1444.
[8]. MacRae, G., et al. (2013)."Slab Effects on Beam-Column Subassemblies—Beam Strength and Elongation Issues." Composite Construction in Steel and Concrete VII, 77-92.
[9]. Green, T.P., et al. (2004). "Bidirectional tests on partially restrained, composite beam-to-column connections." Journal of Structural Engineering, 130(2), 320-327.
[10]. Chaudhari, T., et al. (2019). "Experimental behaviour of steel beam-column subassemblies with different slab configurations." Journal of Constructional Steel Research, 162, 105699.
[11]. MacRae, G. and C. Clifton (2013)."Low Damage Design of Steel Structures." Steel Innovations, SCNZ.
[12]. EN1998-1 (2004). "Eurocode 8: Design of structures for earthquake resistance - Part 1: General rules, seismic actions and rules for buildings", European Committee for Standardization, B-1050 Brussels.
[13]. Mago, N. and C.G. Clifton (2008). "Investigation of the slab participation in moment resisting steel frames (HERA report R 4-140)." New Zealand Heavy Engineering Research Association, Manukau City, New Zealand.
[14]. Leon, R.T., et al. (1998). "Seismic response of composite moment-resisting connections. I: Performance." Journal of Structural Engineering, 124(8), 868-876.
[15]. Hobbs, M. (2014). "Effects of Slab-Column Interaction in Steel Moment Resisting Frames with Steel-Concrete Composite Floor Slabs." Master Thesis, University of Canterbury, Christchurch, New Zealand.

[16]. Chaudhari, T. (2018). "Seismic performance evaluation of steel frame building with different composite slab configurations." Doctor of Philosophy in Civil Engineering Ph.D. Thesis, University of Canterbury, Christchurch, New Zealand.
[17]. Webb, G., et al. "Column Moment Demands from Orthogonal Beam Twisting." Proc., Key Engineering Materials, Trans Tech Publ, 259-269.
[18]. Chaudhari, T., et al. (2015)."Composite slab effects on beam-column subassembly seismic performance." STESSA 2015, China Architecture & Building Press.
[19]. Yamada, S., et al. (2009). "Full scale shaking table collapse experiment on 4-story steel moment frame: Part 1 outline of the experiment." Behaviour of Steel Structures in Seismic Areas: STESSA 2009, 125.
[20]. Chaudhari, T.D. and G.A. MacRae (2016). "Selection of gap infill material for structural seismic applications." Journal of the Structural Engineering Society of New Zealand Inc (SESOC), 29(01).
[21]. Uang, C.-M. and C.-C. Fan (2001). "Cyclic stability criteria for steel moment connections with reduced beam section." Journal of Structural Engineering, 127(9), 1021-1027.
[22]. FEMA451 (2006). "NEHRP recommended provisions: design example." National Institute of Building Sciences, Washington, D.C.
[23]. MacRae, G. and G. Clifton "NZ research on steel structures in seismic areas." Proc., 8th International Conference on Behavior of Steel Structures in Seismic Areas, STESSA, Shanghai, China, p44-58.
[24]. ANSI/AISC:341-10 (2010). "Seismic provisions of structural steel buildings", American Institute of Steel Construction, Chicago, Illinois, USA.
[25]. NZS3404:Part1:1997 (2007). "Steel structures standard part 1-Incorporating amendment no 1 and no 2", Standards New Zealand, Wellington.
[26]. Umarani, C. and G. MacRae (2007). "A new concept for consideration of slab effects on building seismic performance." Journal of Structural Engineering, Structural Engineering Research Centre, Chennai, India, (34-3), 34.
[27]. Kim, J., et al. (2004). "Effect of beam growth on reinforced concrete frames." Journal of Structural Engineering, 130(9), 1333-1342.
[28]. Kattner, M. and M. Crisinel (2000). "Finite element modelling of semi-rigid composite joints." Computers & Structures, 78(1), 341-353.
[29]. Rassati, G.A., et al. (2004). "Component modeling of partially restrained composite joints under cyclic and dynamic loading." Journal of Structural Engineering-ASCE, 130(2), 343-351.
[30]. ENV1993-1-1 (1992). "Eurocode 3: Design of steel structures – Part 1.1: General rules and rules for buildings", European Committee for Standardization, B-1050 Brussels.
[31]. Carr, A. (2004). "Ruaumoko 2D–Inelastic dynamic analysis." Department of Civil Engineering, University of Canterbury, Christchurch.
[32]. Elghazouli, A., et al. (2008). "Seismic performance of composite moment-resisting frames." Engineering structures, 30(7), 1802-1819.
[33]. Ikhlas S. Sheet, et al. (2013). "Modeling of Steel Beam-Column Connections under Dynamic Excitation." Journal of Structural Engineering, published by CSIR-Structural Engineering Research Centre, Chennai, 40(13), 254-261.
[34]. ComFlor80 (2014). "Product guide ComFlor80, available at "http://www.comflor.co.nz/wp-content/uploads/ComFlor/Brochures/ComFlor80Brochure.pdf"." (13 January 2014).
[35]. CSI Berkeley, U. (2015). "Analysis reference manual." SAP2000 V17.2.0.
[36]. AS/NZS:2327 (2017). "Composite structures - Composite steel-concrete construction in buildings", Standards New Zealand, Wellington.
[37]. Aslani, F. and R. Jowkarmeimandi (2012). "Stress-strain model for concrete under cyclic loading." Magazine of Concrete Research, 64(8), 673-685.
[38]. Carreira, D.J. and K.H. Chu (1985). "Stress-strain relationship for plain concrete in compression." Journal of the American Concrete Institute, 82(6), 797-804.
[39]. NZS3101:1 (2006). "Concrete structures standard: Part 1 - The design of concrete structures", Standards New Zealand, Wellington.
[40]. Ribeiro, F.L.A., et al. (2015). "Deterioration modeling of steel moment resisting frames using finite-length plastic hinge force-based beam-column elements." Journal of Structural Engineering, 141(2).
[41]. Ibarra, L. and H. Krawinkler (2005). "Global collapse of frame structures under seismic excitations." John A. Blume Earthquake Engineering Center Technical Report 152, Stanford University

[42]. Kawashima, K., et al. (1992). "The strength and ductility of steel bridge piers based on loading tests." Journal of Research, Japan, 29.
[43]. EC4 (2004). "Eurocode 4: Design of composite steel and concrete structures - Part 1-1: General rules and rules for buildings", European Committee for Standardization, B-1050 Brussels.
[44]. Lam, D. and E. El-Lobody (2005). "Behavior of headed stud shear connectors in composite beam." Journal of Structural Engineering-ASCE, 131(1), 96-107.
[45]. Hicks, S. (2011). "Design resistances of 19 mm diameter headed stud connectors through-deck welded within the ribs of Comflor 60 and Comflor 80 profiled steel decking." HERA, Manukau City, New Zealand, (Received through private communication from Steve Stickland).
[46]. Johnson, R.P. and N. Molenstra (1991). "Partial shear connection composite beams for buildings." Proceedings of Institute of Civil Engineers, Part 2, 679-704.
[47]. Wang, Z. and W. Tizani (2010). "Modelling techniques of composite joints under cyclic loading." In Computing in Civil and Building Engineering, Proceedings of the International Conference, (Nottingham University Press, Nottingham, UK), Paper 254, p. 507.
[48]. Mander, J.B., et al. (1988). "Theoretical Stress-Strain Model for Confined Concrete." Journal of Structural Engineering, 114(8), 1804-1826.
[49]. ACI (2001). "ACI T1.1-01: Acceptance criteria for moment frames based on structural testing", American Concrete Institute.